^{1}H NMR Relaxation Study of Chain Motions and Solid-State Ordering in Stiff, Random Copolymers

Michael Gentzler and Jeffrey A. Reimer*

Center for Advanced Materials, Lawrence Berkeley National Laboratory, and Department of Chemical Engineering, University of California at Berkeley, Berkeley, California 94720-1462

Received July 25, 1996; Revised Manuscript Received September 29, 1997[⊗]

ABSTRACT: Fully-aromatic, thermotropic, liquid crystalline random copolyesters of 4-hydroxybenzoic acid (HBA) and 6-hydroxy-2-naphthoic acid (HNA) were studied at elevated temperatures with ^{1}H NMR. Proton T_1 measurements provide high-frequency characterization of the glass transition. Proton rotating frame relaxation time ($T_{1\rho}$) measurements near room temperature are sensitive to HBA rotational motions; these motions are expected when there is monomer length-scale chain conformational disorder. In melt-quenched samples, this disorder is spatially homogeneous (i.e., the material solidifies without crystallization). Annealing below the nominal solidification temperature (T_s) results only in a slight, uniform lessening of this disorder. For samples annealed above T_s, proton $T_{1\rho}$ measurements show a spatially distinct component in which monomeric rotational motions are suppressed. Spin−diffusion experiments indicate this component has a mean thickness of 10 ± 2 nm. ^{1}H-^{13}C (cross polarization-magic-angle spinning) CP-MAS measurements indicate that these ordered regions are enriched in HBA. The fraction and HNA content of the "cocrystallites" *decrease* at higher annealing temperatures. We discuss a new conceptual model of solid ordering in highly sequence-frustrated, stiff HBA/HNA copolyesters that is consistent with these and previously reported data.

Introduction

Main-chain liquid crystalline polymers (LCPs) are of fundamental interest because they are characterized by complex structures that exist on many length scales: mesoscopic nematic domains, an unusual crystalline morphology, and a micromacroscopic fibrillar texture. These structures are strongly affected by processing in the melt or solid state, and ultimately have a significant impact on final LCP properties. Improved understanding of such structures is essential if the technological promise of these LCPs is to be realized.

The nematic character of LCPs has been conceptualized in terms of rigid-rod models, such as the Doi constitutive model.[1] These idealizations assume a monodomain, nematic fluid phase at equilibrium; such a textureless fluid may only by consistent with LCPs undergoing flow at high deformation rates.[1,2] Most main-chain LCPs (both thermotropes and lyotropes) are only semirigid (i.e., worm-like[3]), with persistence lengths much greater than a monomer length, but much less than the average chain length. This limited chain flexibility, along with disordered molecular structure, polydispersity, and nematicity, may lead to the characteristic hierarchical structures observed in practice.

The presence of all these structural features in main-chain LCPs has made the connection between molecular architecture and useful material properties an elusive goal.[4] Subtle changes can drastically affect properties relevant to processing and solid-state application. For aromatic copolyesters [such as those comprised of 4-hydroxybenzoic acid (HBA) and 6-hydroxy-2-naphthoic acid (HNA)], a low-melting, nematic liquid crystalline state was obtained by *random* copolymerization of structurally different (kinked or flexible) monomers.[5] This "quenched" chain disorder is thought to frustrate short-range ordering of the polymer chains and produce low melting temperatures of ∼300 °C[6] for the HBA/HNA copolymer system compared with ∼450 °C for the HBA and HNA homopolymers[7]. For poly(HBA/HNA), this molecular design strategy also produced an undesirable a low softening temperature. Fortunately, solid-state annealing, especially near the melting point, has been shown to increase poly(HBA/HNA) modulus,[8,9] presumably from a constrained local ordering process.

The "crystallization" (and softening) of HBA/HNA copolyesters is not well understood,[10] despite many previous structural studies. Of particular interest are recent X-ray scattering studies[11−13] in which the authors conclude that some smectic order is present in the LCP melt. The relevance of this order to solidification processes, particularly the "fast crystallization" process of poly(HBA/HNA), was speculated.

Nuclear magnetic resonance (NMR) is a molecular level technique that is complimentary to scattering experiments; it is sensitive to dynamic disorder (due primarily to slower measurement time scales), and uniform signals are obtained from the entire material. Because NMR relaxation times *indirectly* probe for ordered units to the extent that they are characterized by differing motional dynamics,[14] we hope to be able to further characterize the recently proposed melt and near-melt structures. We therefore undertook a complete study of the proton NMR relaxation times in the HBA/HNA system with the goal of determining the extent and character of crystallinity in the poly(HBA/HNA) system. These results are also anticipated to aid future investigations; for example, proton NMR time constants are especially important for exploitation of multidimensional NMR methods aimed at elucidating other structural,[15] orientational, and dynamical properties of polymers.[16]

Our results can be summarized as follows. With the use of elevated pressure and controlled atmospheres over our polymer samples, we obtained reproducible NMR measurements at temperatures in excess of 300 °C. The temperature dependence of ^{1}H spin−lattice (T_1) relaxation times, for 73/27 and 30/70 poly(HBA/HNA), provide a measurement primary glass transition temperature at 140 MHz.

Most of our results derive from the temperature dependence of ^{1}H rotating frame ($T_{1\rho}$) relaxation times

[⊗] Abstract published in *Advance ACS Abstracts,* December 15, 1997.

S0024-9297(96)01109-6 CCC: $14.00

for 73/27 poly(HBA/HNA). We establish $T_{1\rho}$ is sensitive to HBA rotational motions near room temperature, and these motions are quenched in the crystalline regions of poly(HBA). Thus, in both the HBA homopolymer and HBA/HNA copolymer, these HBA motions indicate local conformational disorder in otherwise glassy, noncrystalline regions.

Surprisingly, the $T_{1\rho}$ data show no features attributable to crystallinity in quenched poly(HBA/HNA), despite the presence of an endotherm in differential scanning calorimetry (DSC) studies. Hence, the "fast crystallization" process appears to be solidification from the nematic state. Annealing below the nominal solidification temperature results in further solidification, or "conformal ordering of persistence lengths".

With annealing above the nominal solidification temperature, $T_{1\rho}$ data indicate spatially localized regions characterized by differing motional dynamics. These regions show suppressed HBA and HNA rotational motions and a composition enriched in HBA, and have thicknesses of ~10 nm [based on ^{1}H-^{13}C cross-olarization-magic-angle spinning (CP-MAS) and ^{1}H spin−diffusion measurements, respectively]. The fraction and HNA content of these rigid regions decreases with annealing temperature.

These observations are interpreted in terms of observed "crystallinity" in LCPs and have implications for models of solid-state ordering and rheology in main-chain LCPs.

Experimental Section

The two random[17] copolyesters, 73/27 (Vectra-A900) and 30/70 poly(HBA/HNA), were supplied by the Hoechst Celanese Corporation. Poly(HBA) was supplied by IBM. NMR samples were dried under vacuum (< 0.1 torr) at 120−130 °C for 36 h prior to use.

All spectra were obtained on a home-built solid-state NMR spectrometer operating at 99.7 MHz for ^{1}H resonances. A home-built static VT-probe, used for all ^{1}H measurements, kept samples contained within the NMR coil, but exposed to a 10 atm He or dry nitrogen atmosphere to suppress off-gassing and molten sample foaming. A nominal 90° pulse of 3 μs, a ringdown delay of 4 μs, and a 1-μs dwell time was used for these experiments. The recycling delay was set to 4−5 x T_1 for all measurements except for T_1 measurements, in which a delay of at least 10 x T_1 was used. For $T_{1\rho}$ measurements, a 50 kHz spin−locking field was employed; slight, but negligible, amplifier pulse droop was observable above 30 ms spin−lock times with adamantane. All inversion recovery and spin−locking data were obtained with quadrature phase cycling at each of the randomly selected time increments; intensities were obtained by averaging the first five points of the summed free induction decay signal components. For the spin−diffusion experiment, magnetization was stored for a variable mixing time by a 90° pulse, after a 20-ms spin−lock; a full $T_{1\rho}$ measurement then followed. Each mixing time decay measurement was repeated three times and averaged. Intensity due to spin−lattice relaxation during the mixing time is reduced by alternating the storage direction.

A measure of poly(HBA/HNA) composition is the relative area of the HNA and HBA ether-ring carbon peaks in a ^{13}C MAS spectrum. (See Figure 10.) These two peaks overlap slightly, but are well resolved from the carbonyl and other aromatic peaks,[15] and a simple two-peak, least-squares fit yields a composition. With ^{1}H-^{13}C CP following a ^{1}H spin−locking period, the composition of the ^{1}H reservoir during a $T_{1\rho}$ decay can be followed. A 7-mm Doty VT-MAS probe was used for CP-MAS at 60 °C. Suitably resolved spectra (with negligible spinning sidebands) were obtained with the following conditions: a ^{1}H 90° pulse of 2.5 μs, 50 kHz CP with a 1-ms contact time, 50 kHz ^{1}H decoupling, and 2.8−3.2 kHz MAS spinning speed. In addition to quadrature phase cycling, the ^{1}H 90° pulse and receiver phase were alternated for all spin−lock decay and CP-MAS measurements.

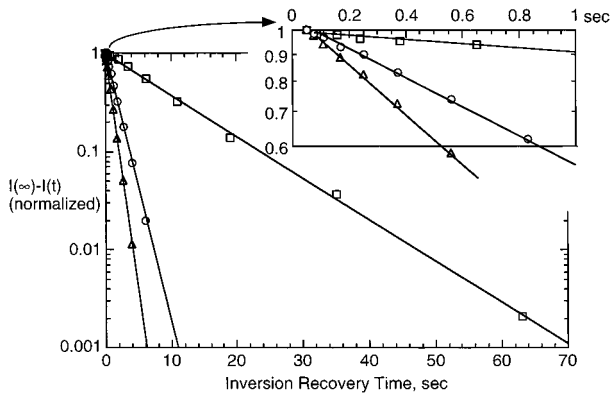

Figure 1. ^{1}H spin−lattice relaxation in Vectra-A900 for three temperatures: 23 °C (open squares), 190 °C (open triangles), 290 °C (open circles). Solid lines are fits to a single exponential decay.

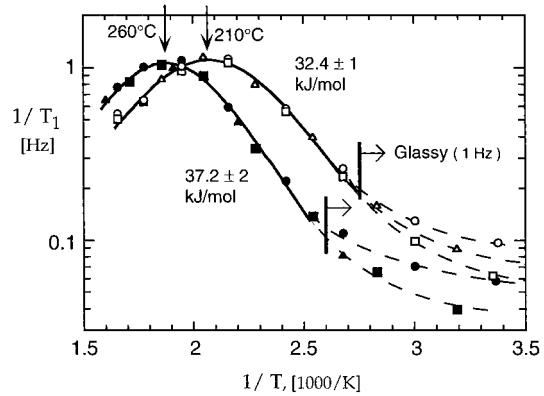

Figure 2. ^{1}H spin−lattice relaxation rate versus inverse temperature for 30/70 poly(HBA/HNA) (filled symbols) and Vectra-A900 (open symbols). Three-stepped temperature ramps (followed by rapid cooling) for each sample are indicated by the circle, square, and triangle, respectively. Solid lines are fits to eq 1, and dashed lines are hand drawn to indicate hysteresis.

With the exception of $T_{1\rho}$ measurements on oriented pellets, all samples are prepared without net director alignment. Polymer pellets were ground and premelted in the NMR probe outside of the magnet at 320 °C at 10 atm for 20 min, followed by rapid cooling. All data were acquired during discrete temperature ramps *in situ*. For all measurements, the time spent at any temperature >140 °C was rarely >1 h; the only exceptions were for a few T_1 measurements and for annealing. The total time at elevated temperatures for some samples may have been many hours; multiple experiments indicated no effects from sample degradation. The ^{1}H probe background signal was checked at room temperature prior to and following all measurements involving sample melting. The broad, featureless background signal was always <0.5% of the sample signal and usually <0.25%. Also, for all measurements, polymer samples were centered in, and much smaller than, the radio-frequency (*rf*) coil; this maximizes *rf* homogeneity throughout the sample.

Results

Figure 1 shows representative inversion recovery difference decays for Vectra-A900 (73/27 HBA/HNA) at various temperatures. All decays were fit to within 1% of the total signal by a single exponential. The temperature dependence of the resulting spin−lattice relaxation rate is shown in Figure 2 for Vectra-A900 and 30/70 poly(HBA/HNA).

Numerous repeated experiments with different Vectra-A900 samples indicated that above the nominal

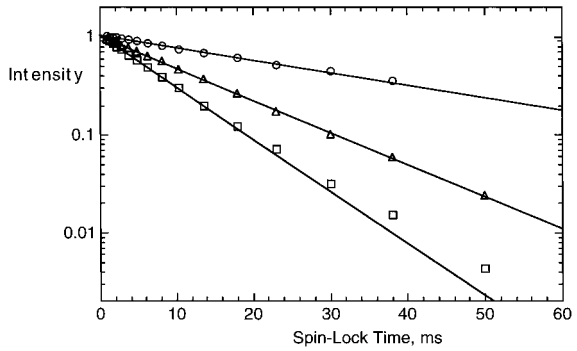

Figure 3. ^{1}H spin−lock relaxation in Vectra-A900 for several temperatures: 21 °C (open squares), 160 °C (open triangles), 300 °C (open circles). Solid lines are fits to a single exponential.

glass transition temperature (∼110 °C for Vectra-A900), the relaxation rate was not affected by sample domain alignment, crystallinity, or thermal history. In this regime, the temperature dependence is characteristic of a single-activated process with correlation time, $\tau_c = \tau_0 e^{E_a/RT}$, for which the relaxation rate will be[18]:

$$\frac{1}{T_1} \propto \frac{\tau_0 e^{E_a/RT}}{1 + (2\pi\nu_0\tau_0 e^{E_a/RT})^2} + \frac{2\tau_0 e^{E_a/RT}}{1 + (4\pi\nu_0\tau_0 e^{E_a/RT})^2} \quad (1)$$

At the relaxation rate maximum, the characteristic frequency of the process is approximately equal to $\sqrt{2}$ times the Larmor frequency, ν_0, or 140 MHz for these data. A least-squares fit to the data above the nominal glass transition temperature gives an activation energy of 32.4 ± 1.0 kJ/mol and a maximum relaxation rate of 1.11 ± 0.02 s^{-1} at 210 ± 2 °C. For the 30/70 poly(HBA/HNA), the similar temperature dependence yields an activation energy of 37.2 ± 1.5 kJ/mol and a maximum relaxation rate of 1.07 ± 0.02 s^{-1} at 259 ± 2 °C.

Below the nominal glass transition, the spin−lattice relaxation is slow, depends very weakly on temperature, and shows a small dependence on cooling rate. In this region, we surmise that relaxation is primarily due to either vibrational motions, allowed by poor chain packing, or impurities such as residual catalyst, free radicals, or dissolved oxygen. These data are included for completeness only and they are not key to the rest of this study.

Figure 3 shows representative ^{1}H spin−lock relaxation decays for powder Vectra-A900 samples at various temperatures. All decays were slightly nonexponential, as detailed in Figure 3. An effective $T_{1\rho}$ constant could be derived from the first 10 ms of the magnetization decay; the temperature dependence of this time constant is shown in Figure 4.

Measurements were also made on as-received extruded Vectra-A900 pellets; these samples have a moderate degree of residual alignment.[19] Figure 5 shows the effective $T_{1\rho}^{-1}$ rate variation when changing the orientation of the pellet (flow alignment) axis with respect to the static field. At 60 °C, and to a lesser extent at 160 °C, relaxation is fastest with chain axes perpendicular to the magnetic field. This is consistent with relaxation dominated by fluctuating *intermolecular* dipolar couplings, transverse to the chain axis. Limited measurements on more highly oriented films at 60 °C showed a similar relaxation rate anisotropy factor of 1.3−1.4. Above 180 °C, the relaxation rate is independent of temperature, showing an orientational anisotropy consistent with relaxation via translational diffusion or director fluctuations.[20]

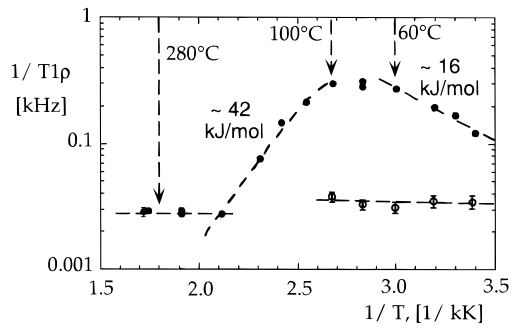

Figure 4. ^{1}H spin−lock relaxation rate for Vectra-A900 powder (filled symbols) versus inverse temperature. The dashed lines are hand drawn to indicate regions with different relaxation mechanisms. The relaxation rate of the crystalline component of Vectra-A900, annealed at 285 °C, is shown with open symbols.

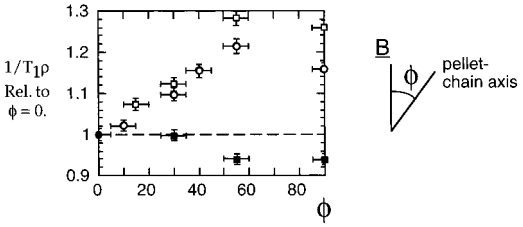

Figure 5. ^{1}H spin−lock relaxation rate for Vectra-A900 pellets at 60 °C (open squares), 160 °C (open circles), and 309 °C (filled squares), versus angle between the alignment axis and the magnetic field.

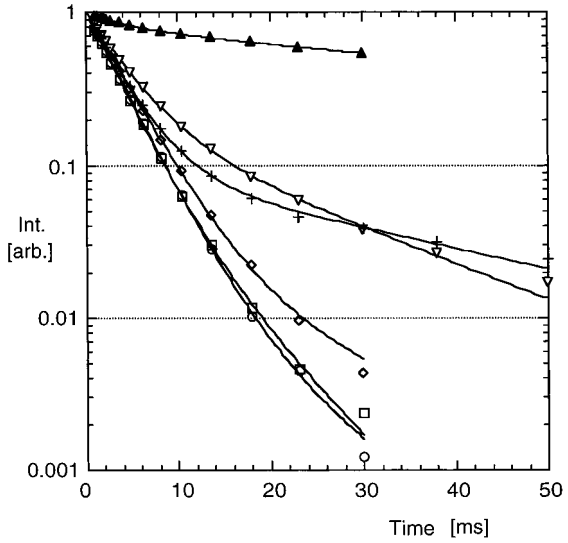

Figure 6. ^{1}H spin−lock relaxation decay, at 60 °C, for poly(HBA) (filled triangles) and Vectra-A900 powder that was premelted (open circles), annealed 1 day at 225 °C (open diamonds), annealed 1 day at 225 °C and remelted (open squares); annealed 16 h at 255 °C (open triangles); and annealed 6 h at 285 °C (crosses).

The effect of "crystallization" on the relaxation decay at 60 °C is shown in Figure 6. A Vectra-A900 powder sample was (1) premelted at 320 °C for 20 min, (2) annealed at 225 °C for 26 h, and (3) remelted. After each of these steps the sample was cooled rapidly to 60 °C for a $T_{1\rho}$ measurement. Additional samples were similarly treated, except for annealing at either 255 °C for 16 h or 285 °C for 6 h. ($T_{1\rho}$ decays obtained after melting steps were virtually identical for all samples; data are shown only for the sample annealed at 225 °C.)

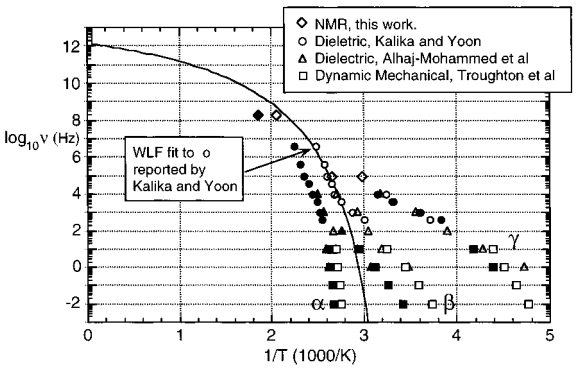

Figure 7. Compiled map of relaxation processes in 73/27 (open symbols) and 30/70 (closed symbols) poly(HBA/HNA).

Finally, the $T_{1\rho}$ decay of poly(HBA), presumably highly crystalline,[21] is also shown.

Discussion

Our discussion of the data is divided into two parts. First, we use the temperature dependence, extrapolated activation energies, and magnitudes of the T_1 and $T_{1\rho}$ relaxation times to argue that the molecular phenomena associated with these relaxation times are HBA/HNA ring flips and a classic, nonspecific glass transition. The focus of these arguments will be Figures 2 and 4; Figure 7 is the penultimate interpretive figure. Our second phase of analysis presents the interpretation of $T_{1\rho}$ data in terms of "crystallinity." Figure 6 will be the focus of this section, with Figure 11 representing the denouement.

The Mechanisms for T_1 and $T_{1\rho}$ Relaxation. Proton spin−lattice relaxation in polymeric materials is due to stochastic molecular motions that produce local fluctuating magnetic fields via the proton homonuclear dipolar interaction. There are three possible molecular motions giving rise to the observed spin−lattice relaxation in poly HBA/HNA; they are, molecular reorientation, translational diffusion, and thermal fluctuations of the liquid crystalline director. Director fluctuations are not considered because these systems are characterized by high viscosities (>1 P), even in the melt at 350 °C[20]; thus, the cutoff frequency for nematic fluctuations is undoubtedly far below the Larmor frequency (∼140 MHz) that characterizes spin−lattice relaxation. Translational motion is not likely to be active below the melting point because of crystallinity and the rigidity of the molecules "tied" between crystallites.[22] We turn our attention, therefore, to relaxation due to molecular reorientations.

Based on previous work,[23−28] three distinct ^{1}H NMR homonuclear dipolar relaxation mechanisms involving molecular reorientations might be observable; they are, crankshaft rotational motion of HNA units, rotational motion of HBA units, or a classic, nonspecific glass transition. (A fourth conceivable motion, rotation of the HBA phenyl ring about its *para*-axis, appears to be linked with the onset of HBA rotational motion, as seen by dielectric and mechanical loss measurements.[28]) We believe the relaxation mechanism is a primary glass transition associated with the onset of large scale correlated chain motions, including rotational motions of both HBA and HNA units.

Figure 7 shows a plot of frequency versus reciprocal temperature for various transitions in poly(HBA/HNA) compiled from the literature[29] and the relaxation peaks given in Figures 2 and 4. The NMR T_1 peaks from Figure 2, shown as diamonds in Figure 7, are obviously in good agreement with those predicted for the combined α, β, and γ transitions seen at frequencies >1 MHz.[23] These transition includes large-scale correlated chain motions (the α transition), as well as rotational motions of the HBA units (the γ transition) and HNA units (the β transition). The magnitude of the T_1 activation energy, however, is lower than that expected from the slope of the master plot given in Figure 7 or those reported in the literature.[23,24] This discrepancy is expected because, in general, the shape of the NMR relaxation rate−temperature dependence will underestimate the true activation energy of the process because of the presence of multiple time scales. In dielectric relaxation measurements, a similar many-body relaxation problem is also encountered.[32]

Proton rotating frame relaxation ($T_{1\rho}$) in polymeric materials is characterized by motion on the timescale of twice the inverse of the field-locking frequency; in our case this would be 100 kHz. Figure 7 also shows the peak temperatures derived from the $T_{1\rho}$ data given in Figure 4; agreement with other transition measurements is excellent. We note that $T_{1\rho}$ relaxation governed by glass transition mechanisms is also consistent with the orientation dependence of the relaxation rate at 60 and 160 °C (Figure 5). In poly(HBA/HNA), HBA or HNA rotational motions will produce fluctuations of primarily *intermolecular* dipolar couplings. The static homonuclear dipolar Hamiltonian is proportional to $(3\cos^2\theta - 1)$, where θ is the angle between the interproton vector of interest and the static magnetic field. Because the largest *intramolecular* couplings, between adjacent protons on aromatic rings, are oriented approximately parallel to the chain axis, these couplings are not significantly modulated by chain rotational motions. On the other hand, *intermolecular* couplings are on average, transverse to the chain axis; therefore, orienting the chain axis perpendicular to the static magnetic field should maximize the fluctuation amplitude of the average intermolecular dipolar field and the resulting $T_{1\rho}$ relaxation rate. Additionally, note that the greater orientation dependence at 60 °C is consistent with relaxation being dominated by HBA rotational motions, which should be more anisotropic than the combined HNA and long-range (isotropic) glass transition probed at 160 °C.

Figure 4 shows that $T_{1\rho}$ relaxation is characterized by different activation energies on either side of a flat-topped maximum; this suggests that eq 1 must be replaced by a model that includes two independent time constants; a simple sum of two BPP-type peaks[18] would account for the data. This concept is easily understood noting that both the β and γ glass relaxations are contributing to the observed relaxation, with overlapping BPP-peaks near 100 and 60 °C. The important implication is that depending on the choice of measurement temperature, $T_{1\rho}$ measurements can probe either HBA or HNA rotational motions. Note also that the apparent activation energies/slopes on either side of the overlapping maxima in Figure 4 are much smaller than the true peak process activation (from Figure 7). Therefore, as with the spin−lattice relaxation, a significant degree of disorder in Vectra-A900 likely produces a distribution of correlation times.

The $T_{1\rho}$ relaxation data are slightly nonexponential (Figure 3). A fraction of this nonexponential behavior is almost certainly due to the rate dependence on chain director orientation. Our experiments show that this

Table 1. Biexponential Curve-Fit Results for Spin−Lock Relaxation at 60 °C

sample	thermal history	short $T_{1\rho}$[a]	long $T_{1\rho}$[b]	short component fraction
poly(HBA)	unknown	4.3 ± 0.3	75 ± 2.5	0.19 ± 0.01
Vectra-A900 #1	quenched from melt	3.4 ± 0.07	7.7 ± 1.2	0.92 ± 0.03
	annealed at 225 °C, 24 h	4.0 ± 0.15	15 ± 20	0.97 ± 0.04
	remelted and quenched	3.6 ± 0.07	11 ± 7	0.98 ± 0.02
Vectra-A900 #2	quenched from melt	3.5 ± 0.25	7.5 ± 2.0	0.85 ± 0.11
	annealed at 255 °C, 16 h	4.1 ± 0.1	17.3 ± 1.2	0.78 ± 0.02
	remelted and quenched	3.5 ± 0.25	9 ± 3	0.87 ± 0.10
Vectra-A900 #3	quenched from melt	3.3 ± 0.08	8.5 ± 0.9	0.88 ± 0.03
	annealed at 285 °C, 6 h	3.6 ± 0.06	32 ± 4	0.90 ± 0.01
	remelted and quenched	3.5 ± 0.14	7.5 ± 1.5	0.93 ± 0.05
Vectra-A900 #4	quenched from melt			
	annealed at 255 °C, 16 h; 285 °C, 6 h	3.5 ± 0.06	31 ± 3	0.89 ± 0.01

[a] ms. [b] ms.

behavior could modify $T_{1\rho}$ by a maximum of ∼40%. Table 1 shows, however, that biexponential fits to the relaxation data yield minority component $T_{1\rho}$ values that are 200−400% of the majority component. It appears, then, that $T_{1\rho}$ nonexponentiality is due to spatial variations in relaxation rate that are smoothed by spin−diffusion during spin−locking (vide infra). This conclusion is consistent with the disorder-induced distribution of correlation times governing the apparent activation energies for T_1 and $T_{1\rho}$.

Crystallinity in Poly(HBA/HNA). Because of its sensitivity to molecular motion at kilohertz frequencies, $T_{1\rho}$ relaxation can be an important probe of crystallinity in polymers. The reduced mobility associated with the formation of crystallites usually leads to reduced motion and a corresponding decrease in the rate of $T_{1\rho}$ relaxation. This is clearly demonstrated in Figure 6, along with the analyses given in Table 1, for poly(HBA). The strongly biexponential decay at 60 °C clearly indicates that the poly(HBA) is 80% crystalline; we associate the very long $T_{1\rho}$ with a substantial lack of molecular motion in the crystalline component. The short $T_{1\rho}$ component is attributed to noncrystalline material in which enough local conformational disorder exists to allow HBA rotational motion. With this in mind, we undertook a study of $T_{1\rho}$ as a function of thermal history in Vectra, on the assumption that we would see "crystallite" formation. The results are surprising.

First, consider the effect of annealing at 225 °C, as shown in Figure 6 and Table 1. For Vectra-A900 the majority, short-time $T_{1\rho}$ component increased from 3.4 to 4.0 ms with annealing at 225 °C, and returns to 3.6 ms upon remelting. With the same annealing protocol and with $T_{1\rho}$ measurements at 130 °C, qualitatively similar behavior is observed, but the reversible change in relaxation rate was smaller and positive (5 ± 3% versus −10 ± 6% at 60 °C). These changes in relaxation with annealing at 225 °C are quite small, suggesting a slight slowing of HBA and HNA rotational motions. According to the heuristics of BPP theory,[18] at 60 °C, below the relaxation rate maximum temperature, a "freezing" of HBA motion should increase $T_{1\rho}$; and at 130 °C, above the maximum, a "freezing" of HNA motion should decrease $T_{1\rho}$. The trends in the data are consistent with these heuristics.

The $T_{1\rho}$ relaxation at 60 °C is dominated by HBA rotational motions, so comparison with the strongly biexponential decay of poly(HBA) in Figure 6 is possible. The short-time $T_{1\rho}$ constant, associated with ≈97% of the magnetization, matches that for the disordered region of poly(HBA); there is no evidence whatsoever of classic crystallinity either before or after the 225 °C anneal! The 225 °C annealed 73/27 poly(HBA/HNA) appears to be a "well-solidified nematic", suggesting that the significant transition enthalpy observed for material annealed at or below 225 °C[6] must be associated with nonspecific interactions arising from improved chain packing.

After annealing at 255 °C, a significant (≈20%) long-time $T_{1\rho}$ component is present. The magnitude of $T_{1\rho}$, 17 ms ($T_{1\rho}^{-1} = 0.06$ kHz), suggests the formation of an ordered domain in which aromatic ring flips are suppressed. This suggestion is confirmed by measurements on a sample that was annealed at 285 °C, for which the ordered component shows an even slower rate of 0.033 kHz; this rate is virtually independent of temperature between 22 and 100 °C, as seen in Figure 4.

This ordering presumably occurs via translational motion because the chains have significant motional freedom far above the (≈Hz) glass transition at 110 °C. The ordering is also correlated with the change of chain packing from pseudo-hexagonal to orthorhombic.[33] Association of this rigid fraction with "crystallinity", hence, will be quite significant; because, upon changing the annealing temperature from 255 to 285 °C, the apparent rigid fraction *decreases* from 22 to 10% and the relaxation time constant ("order") increases.

Further interpretation of the long-time $T_{1\rho}$ (ordered) component that results from annealing at >225 °C is possible by using proton spin−diffusion measurements.[14] In this experiment, a preparatory 20-ms spin−lock (largely) destroys the magnetization in the disordered domains; during the mixing period, spin−diffusion occurs at a normal rate, and a $T_{1\rho}$ measurement reveals the progressive diffusion of magnetization into the disordered domains. The rate of spin−diffusion can, under some circumstances,[34] yield geometric information and domain size.

Figure 8 shows representative decays for this experiment on the 285 °C annealed Vectra A900 sample. The solid lines indicate biexponential fits with the long-time $T_{1\rho}$ component fixed at 45 ms. Consistently good fits resulted for all mixing times (this was also true for the 255 °C sample for which 19 ms was used.) Figure 9 shows the experimental recovery of the disordered component. Two theoretical models have been fit to these data. The first assumes a regular, periodic arrangement of crystallites in the material. A single thickness, b^*, characterizes the "crystallites" which are planar, square rods or cubes, depending on the dimensionality. The solution for the recovery of the initially depleted component is:

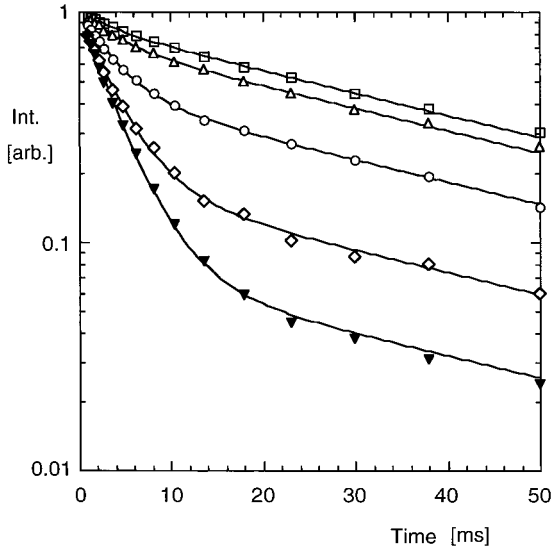

Figure 8. Representative ^{1}H spin−diffusion data. ^{1}H spin−lock relaxation decays, at 60 °C, for Vectra-A900 annealed at 285 °C, at mixing times of 1 ms (squares), 8 ms (triangles), 64 ms (circles), 512 ms (diamonds), and 100 s (filled triangles).

$$M = M_0 + \frac{(M_f - M_0)}{M_f(1 - M_f)} \times \left[\xi^{nd} - \left(\xi^2 + 2\sum_{n=1}^{\infty}\frac{\sin^2(n\pi(1-\xi))}{(n\pi)^2}\exp\left(\frac{-4\xi^2(n\pi)^2 Dt}{b^*}\right)\right)^{nd}\right] \quad (2)$$

where M is the disordered fraction, $M_0 = M(t = 0)$, $M_f = M(t \rightarrow \infty)$, nd is the crystallite dimensionality (1, 2, or 3), D is the diffusion coefficient, t is mixing time, and $\xi = (1 - M_f)^{1/nd}$.

The second model, of Cheung and Gerstein,[35] assumes dilute crystallites with a Poisson distribution of thickness b:

$$P(b) = \left(\frac{1}{b^*}\right)\exp\left(\frac{-b}{b^*}\right) \quad (3)$$

To fit the data, the ^{1}H spin−diffusion constant is needed. Following earlier work,[14,35] we obtain estimates of $D = 0.5 \pm 0.1$ nm^2/ms for 73/27 poly(HBA/HNA). This result is very close to values observed in other solid polymers.[16]

The results of least-squares fits of the two models for one-, two-, and three-dimensional domains are shown in Table 2. The fit was a three-parameter fit for the mean thickness, b^*, and the initial and final disordered fraction (not tabulated). The one-dimensional (1D) Cheung-Gerstein model gives the lowest crystallite thickness of 5.4 nm. However, the squared error for each case indicates better fits are the 1D periodic model and two-dimensional (2D) or three-dimensional (3D) Cheung-Gerstein model, which have mean thicknesses between 11.0 and 19.5 nm, as shown in Figure 9. Similar results results are obtained for the 255 °C sample.

Prior to interpreting these distances, we must first assess whether or not spin−diffusion during the $T_{1\rho}$ measurement significantly confounds our analysis. Under strong spin−locking, ^{1}H spin diffusion will occur at half the normal rate.[34] Thus if the ordered domain size, X_c, is large compared with the length over which diffusion occurs during the $T_{1\rho}$ measurement, X_d, the observed component fraction and time constant properly reflect ordered domain properties. If the domain size is too small, magnetization from the long $T_{1\rho}$ domain "bleeds" into the fast relaxing domains, resulting in a smaller apparent long $T_{1\rho}$ fraction and time constant. Approximating X_d as $\sqrt{D\tau_e n}$, where n is dimensionality and $\tau_e = 10$ ms for the $T_{1\rho}$ experiment, X_d is calculated as 2.2, 3.2, and 3.9 nm for 1-, 2-, and 3D domains, respectively. Taking 10 nm to be a typical crystallite thickness, X_c is thus considerably larger than X_d. These results allow us to view the ordered domains that result from annealing Vectra-A900 at 255 and 285 °C to be significantly sized, ordered regions with $T_{1\rho} = 18 \pm 2$ and 38 ± 10, and fractions of $15 \pm 3\%$ and $8 \pm 2\%$, respectively (based on the spin−diffusion model). These low values agree reasonably well with some previous measurements.[11]

A measurement of the average copolyester composition in these domains can also be made. Table 3, which results from analysis of CP-MAS data represented in Figure 9, shows the apparent fraction of HNA units

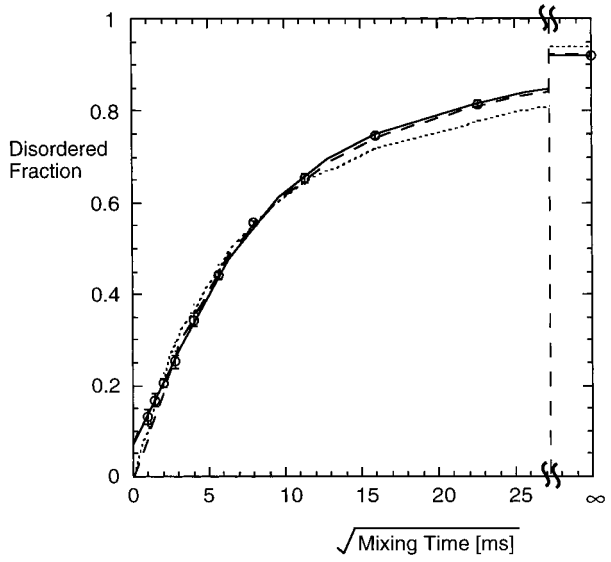

Figure 9. Diffusion of ^{1}H magnetization into the disordered component of Vectra-A900 (annealed at 285 °C). Also shown are least-square fits, assuming a 1D periodic model (solid line), and 2D Cheung-Gerstein (dashed line) and 1D Cheung-Gerstein (dotted) models for the "crystallite" morphology.

Table 2. Spin−Diffusion Recovery Curve-Fit Results

annealing	"crystallite" model[a]	copolymer[b]	mean "crystallite" thickness[c]	least-squares error[d]
255 °C, 16 h	1	periodic	10.3	0.20
	2	periodic	20.0	0.55
	3	periodic	28.4	0.53
	1	random	3.7	0.27
	2	random	9.6	0.09
	3	random	15.7	0.08
285 °C, 6 h	1	periodic	11.0	0.01
	2	periodic	22.5	0.63
	3	periodic	32.1	0.73
	1	random	5.4	0.45
	2	random	12.1	0.06
	3	random	19.5	0.04

[a] # Finite dimensions. [b] Periodic = periodically spaced crystals with fixed thicknesses; random = dilute crystals with exponential thickness distribution. [c] nm, 10% uncertainty. [d] Normalized.

Table 3. CP-MAS Apparent Vectra-A900 Composition during Spin−Lock Relaxation at 60 °C

thermal history	spin−lock decay time, ms[a]	fraction HNA[b]
quenched from melt	1	31 ± 1.8
	2	32 ± 1.6
	4	32 ± 1.5
	10	39 ± 2.3
annealed at 225 °C for 24 h	1	31 ± 1.2
	2	33 ± 1.1
	4	32 ± 1.3
	10	32 ± 1.1
annealed at 255 °C for 16 h	1	27 ± 1.5
	2	30 ± 1.2
	4	28 ± 1.3
	10	23 ± 1.5
	20	21 ± 1.2
annealed at 285 °C for 6 h	1	30 ± 1.1
	2	32 ± 0.9
	4	27 ± 1.2
	10	16 ± 1.0
	20	7 ± 3
annealed at 255 °C for 16 h, followed by 285 °C for 6 h	1	30 ± 1.1
	2	30 ± 1.4
	4	26 ± 1.4
	10	16 ± 1.0
	20	11 ± 2

[a] Includes 1-ms CP period. [b] From relative areas of ether ring-carbon peaks.

versus spin−locking time for quenched and annealed samples. Both quenched and 225 °C annealed samples showed fractions between 31 and 39% HNA for all spin−locking times. This positive deviation from the true composition of 27% is expected. The dominant relaxation centers are rotating HBA units, and spin diffusion between rings is not infinitely fast; thus, HNA units should have a slightly higher ^{1}H polarization (and thus resulting ^{13}C CP signal) throughout the decay. The 255 °C "crystallized" sample shows a lower and decreasing HNA fraction, equal to 21 ± 1.2% after a 20-ms spin−lock (when the ^{1}H magnetization is associated almost entirely in the ordered domains). The 285 °C annealed sample indicates an even lower HNA fraction equal to 7 ± 3%. (These compositions are accurate, given the significantly slower spin−lock decay rate at long times.) Thus, the "crystallites" significantly exclude HNA units. This enhanced HBA content, increasing with annealing temperature, correlates with the increased relaxation time constant (i.e., conformational order) observed.

In summary, we are left with the following results: There is no "classic crystallinity" in Vectra upon annealing at 225 °C. With annealing at 255 or 285 °C, ordered domains appear; however, these have compositions different from the bulk and $T_{1\rho}$ time constants, suggesting a nematic glass with minimal aromatic ring flips. The composition, fraction, and residual molecular motion of these domains change surprisingly with annealing temperature. In our view, the notion of crystallinity seems inappropriate in these materials. A new perspective is needed.

Figure 10 schematically depicts our view of the progression of solid-state order in poly(HBA/HNA), as revealed by our NMR measurements. Ordering processes are driven by conformational entropy minimization given the chemically similar, but structurally different, monomers. Crystallization is frustrated, however, by the random chain sequence. Annealing at increasing temperatures results in a progression of

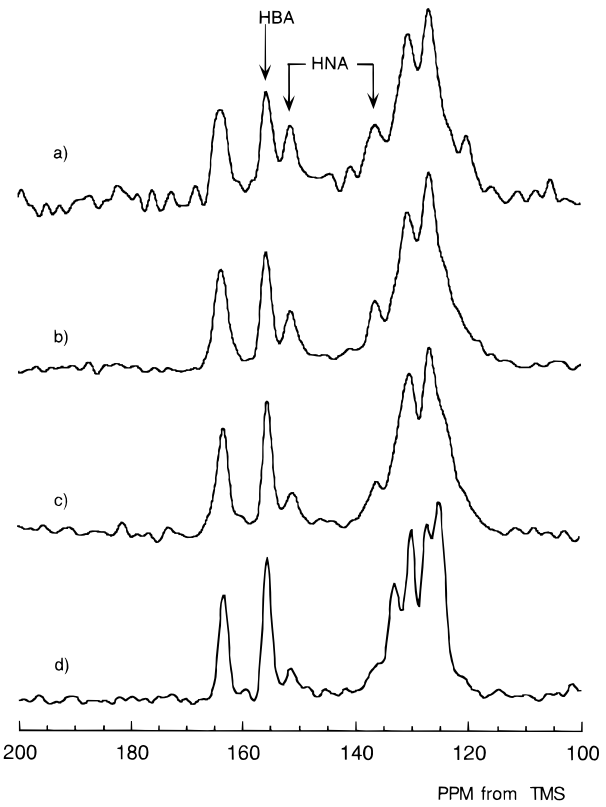

Figure 10. ^{13}C CP-MAS spectra, obtained after 10 ms of ^{1}H spin−locking, for Vectra-A900: (a) quenched; (b) annealed at 225 °C for 24 h; (c) annealed at 255 °C for 16 h; (d) and annealed at 285 °C for 6 h. The arrows indicate well-resolved monomer peaks; the aromatic ring-ether carbons, at 155 and 151 ppm, allowed easy composition determination.

metastable states, superficially analogous to protein folding with many kinetically trapped "misfolded" states.[36,37]

As received, melt-quenched Vectra-A900 is highly disordered; that is, although nominally aligned, the polymer chains are not registered or packed optimally on any length scale. Annealing below some critical temperature (close to the nominal solidification temperature) does not induce crystallinity. The low temperature "slow crystallization" process associated with thermal measurements,[6,22] appears to be further solidification. We infer that translational motion does not occur and crystallization is totally frustrated by poor matching of chain sequences/conformations. The significant DSC peak enthalpy observed[6,22] is due to conformational packing improvements on a length scale of the polymer persistence length, allowed by local chain motion above the glass transition; upon heating, this first-order transition, distinct from the solid−nematic transition, is associated with "melting of persistence lengths."

There are interesting implications of this state. For example, the solidified nematic, lacking any specific lateral interactions between chains, should plastically deform in a slip mode. Indeed, this phenomenon has been observed.[31] It is interesting that scanning (SEM) and transmission electron microscopy (TEM) measurements[11] show a spatially segregated layered microstructure for poly(HBA/HNA) oriented films that have not been annealed above T_s. Based on our results, this morphology must reflect segregated chain conformational distributions, not crystalline domains. Earlier studies have demonstrated meridonal layer peaks on

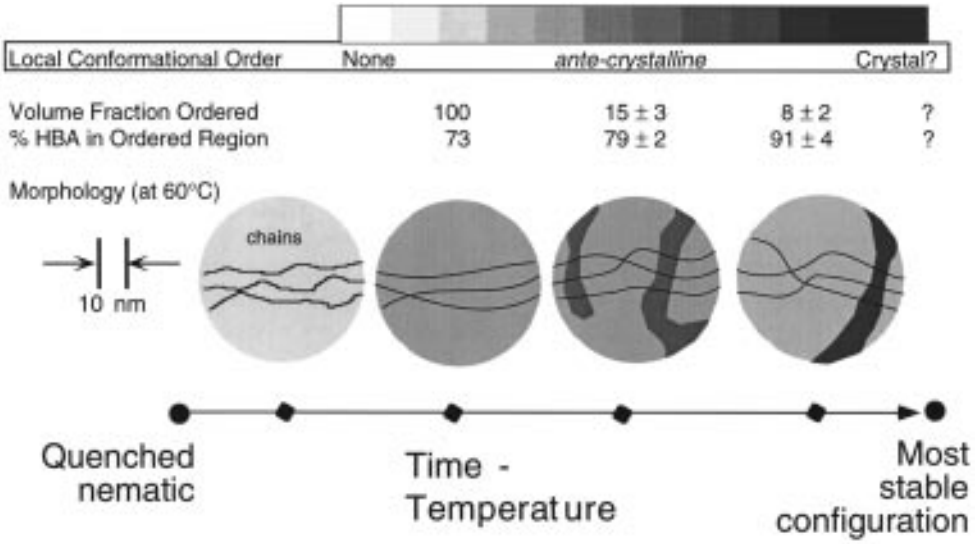

Figure 11. Schematic progression of observed (kinetically trapped) Vectra-A900 solid states: quenched nematic with high conformational disorder; highly sequence-frustrated solid with conformational disorder locally annealed; highly sequence-frustrated solid with conformational disorder globally annealed; same (at higher temperature). Quantitative crystallite composition and abundances are reported.

X-ray fiber diagrams, indicating that limited chain registry exists in the solid state.[12] Recent X-ray studies in the melt also have shown this registry,[13] but the authors emphasize that this registry does not indicate specific monomer sequence registry. These results strongly suggest that "chain registry" is due to conformational matching, which is a natural consequence of the stiff, random chain, along which the excluded volume surface or "chain kinkiness" fluctuates.

A softening of the "solid nematic" state occurs between 225 and 255 °C, probably close to the solidification temperature of 230−235 °C for 75/25 poly(HBA/HNA).[6] Above this temperature, T_s, "cocrystallization-like" ordering occurs. However, 73/27 poly(HBA/HNA) defies categorization as crystalline; characterization of poly(HBA/HNA) as a condis crystal,[6,38] or any other classic type, is clearly inappropriate because the solid-state order is entirely metastable. Above T_s, as annealing temperature increases, the melting enthalpy decreases and the nematic transition temperature increases.[6,22] Also, the volume fraction and HNA content of the conformationally ordered domains decreases with annealing temperature. Thus, the total transition entropy change is decreasing. Solid poly(HBA/HNA) is better characterized as a "sequence-frustrated, ordered nematic solid". The higher temperature ordered states are distinct from those attained below T_s only because chain conformal pattern matching occurs over a much large length scale via activated translational chain motion. In flexible random copolymers, the analogous ordering process is "cocrystallization", for which similar time- and temperature-dependent crystalline compositions have recently been reported.[39,40] We have considered and rejected transesterification in the solid state as an alternative explanation.[41]

In hindsight, the stiffness of the HNA/HBA copolyester greatly affects the ordering behavior and its elucidation. In contrast to flexible polymers, the "ordering unit length scale" is not a monomer, but rather a persistence length of ∼12 nm for 70/30 poly(HBA/HNA).[44] These "ordering units"[45] have a random character, containing ∼15 monomeric units. A continuum of (nonequilibrium) ordered states is not too surprising. It is interesting that observed "crystallite" thicknesses mimic this persistence length scale. Rejecting the 3D crystallite models as unrealistic,[11] our results in Table 2 suggest a fairly narrow distribution of "crystallite" sizes with typical thicknesses of 10 ± 2 nm. Although this range agrees well with 7.3 ± 1.1 nm of Hanna et al., the presence of 10-nm thicknesses (even for the 1D Cheung-Gerstein results), suggests any "crystallite" model based solely on sequence matching is not appropriate.[11,46] The unsatisfactory crystallization models and crystallinities derived from wide-angle X-ray scattering measurements[10] are pathological for stiff polymers. The base-chain alignment and densely packed, rigid monomeric units mask the large-scale dynamic conformational disorder (or lack thereof) clearly evident in dynamic measurements.

Broader understanding of stiff, random copolymers like the HBA/HNA copolyesters will be obtained from fundamental theory or simulation; this should be straightforward because enthalpic effects can be neglected. Many interesting details remain. One might expect segregation of topological defects like chain entanglements (in addition to conformal lengths rich in "undesirable" monomers) into the dynamically disordered domains at high temperatures.[9] For polymers with three or more different monomers, simple prediction of the domain compositions (in globally annealed states) with sequence matching is not obvious.[14,47] Also, it would be nice to confirm that the "fast" crystallization process is solidification, and that the associated weak melting endotherm, always observed, arises from a "mean field" barrier (preventing nonlocalized translational chain motion) that is due to chain alignment only, frozen from the nematic state. Regardless, a larger question is whether the HBA/HNA system behavior is archetypal of stiff, random copolymers and a "limiting case" for copolymers with sequence frustration on short length scales, such as block copolymer blends or molten globular proteins.

Conclusions

Local-chain dynamics in Vectra-A900 have been studied by solid- state ^{1}H NMR spectroscopy. The ^{1}H spin−lattice and ^{1}H spin−lock relaxation was measured from room temperature to >310 °C. From spin−lattice

relaxation at 140 MHz, the glass transition temperatures of Vectra-A900 and 30/70 poly(HBA/HNA) were determined to be 210 and 259. °C, respectively. A compiled master relaxation plot (Figure 7) beautifully demonstrates the physical basis of the phenomenological WLF or Vogel-Fulcher equations for polymeric glasses. The merging of increasingly localized and less thermally activated relaxations with the primary glass transition (at increasing frequencies) gives the apparent decreasing activation energy of the primary glass transition with frequency.

Proton-rotating frame relaxation time ($T_{1\rho}$) measurements near room temperature are sensitive to HBA rotational motions, the presence of which indicate monomer length scale chain conformational (or packing) disorder. Classic crystalline ordering suppresses these rotational motions in poly(HBA). Unless annealed above the nominal solidification temperature, T_s, Vectra-A900 appears dynamically as a *noncrystalline* "quenched nematic", lacking optimized chain registry. In this state, large length scale translational chain motion does not occur; above T_g, however, significant chain axis fluctuation and rotational motion allows for persistence length scale conformational annealing. Above T_s, a spatially distinct rigid component, in which HBA and HNA rotational motions are suppressed, is observed. Spin−diffusion experiments indicate a likely mean domain thickness of 10 ± 2 nm; the smallest possible mean thickness is 4−5 nm. The composition in these ordered regions is enhanced in HBA, as indicated by ^{1}H-^{13}C CP-MAS measurements. The fraction and HNA content of the "cocrystallites" decreases at higher annealing temperatures. These results compliment previous thermal and structural studies indicating that poly(HBA/HNA) forms a (highly) sequence-frustrated nematic solid and it defies characterization as a condis crystal or description by previous models. The solid progresses through a continuum of nonequilibrium states; as temperature is increased, a decreasing fraction of polymer chain segments can conformationally order into a rigid solid state.

Acknowledgment. This work was supported by the Director, Office of Energy Research, Office of Basic Energy Science, Materials Science Division, U.S. Department of Energy, under contract no. DE-AC03-76SF00098. MG gratefully acknowledges an AT&T graduate fellowship. The authors are also grateful to Professor Morton M. Denn for helpful discussions and a critical reading of this manuscript.

References and Notes

(1) Larson, R. G. *Constitutive Equations for Polymer Melts and Solutions*; Butterworth: Boston, 1988.
(2) Mori, N.; Hamaguchi, Y.; Nakamura, K. *J. Rheol.* **1997**, *41*, *in press*.
(3) Brelsford, G. L.; Krigbaum, W. R. In *Liquid crystallinity in polymers*; Ciferri, A., Ed.; VCH: New York, 1991.
(4) *Liquid crystalline polymers*; Report NMAB-453 under National Research Council; National Academy: Washington D.C., 1990.
(5) Donald, A. M.; Windle, A. H. *Liquid crystalline polymers*; Cambridge University: 1992.
(6) Cheng, S. Z. D. *Macromolecules* **1988**, *21*, 2475.
(7) Muhlebach, A.; Lyerla, J.; Economy, J. *Macromolecules* **1989**, *22*, 3741.
(8) Lin Y. G.; Winter, H. H. *Macromolecules* **1988**, *21*, 2439.
(9) Collins, G.; Long, B. *J. Appl. Polym. Sci.* **1994**, *53*, 587.
(10) Langelaan, H. C.; Posthuma de Boer, A. *Polymer* **1996**, *37*, 5667.
(11) Hanna, S.; Lemmon, T. J.; Spontak, R. J.;Windle, A. H. *Polymer* **1992**, *33*, 3.
(12) Biswas, A.; Blackwell J. *Macromolecules* **1988**, *21*, 3152.
(13) Hanna, S.; Romo-Uribe, A.; Windle A. H. *Nature* **1993**, *366*, 546.
(14) Amundson, K. R.; Reimer, J. A.; Denn, M. M. *Macromolecules* **1991**, *24*, 3250.
(15) Tang, P.; Reimer, J. A.; Denn, M. M. *Macromolecules* **1993**, *26*, 4269.
(16) Schmidt-Rohr, K.; Spiess, H. W. *Multidimensional Solid-State NMR and Polymers*; Academic: London, 1994.
(17) Muehlebach, A.; Johnson, R. D.; Lyerla, J.; Economy, J. *Macromolecules* **1988**, *21*, 3117.
(18) Bloembergen, N.; Purcell, E. M.; Pound, R. V. *Phys. Rev.* **1948**, *73*, 679.
(19) ^{1}H NMR lineshape measurements indicated a typical order parameter of 0.3 ± 0.05. See Gentzler, M.; Reimer, J. A.; Denn, M. M. *Polym. Prepr. (Am. Chem. Soc., Div. Polym. Chem.)* **1996**, *37*, 764; Gentzler, M. Ph.D. Dissertation, University of California, Berkeley (1997, in preparation).
(20) Doane, J. W. In *Magnetic Resonance of Phase Transitions*; Owens, F. J., Poole, C. P., Jr., Farach, H. A., Eds.; Academic: New York, 1979; Chapter 4.
(21) Economy, J.; Storm, R. S.; Matkovich, V. I.; Cottis, S. G.; Nowak, B. E. *J. Polym. Sci.* **1976**, *14*, 2207.
(22) Butzbach, G. D.; Wendorff, J. H.; Zimmermann, H. J. *Polymer* **1986**, *27*, 1337.
(23) Kalika, D. S.; Yoon, D. Y. *Macromolecules* **1991**, *24*, 3404.
(24) Alhaj-Mohammed, M. H.; Davies, G. R.; Abdul Jawad, S.; Ward, I. M. *J. Polym. Sci., Polym. Phys.* **1988**, *26*, 1751.
(25) Troughton, M. J.; Davies, G. R.; Ward, I. M. *Polymer* **1989**, *30*, 58.
(26) Fyfe C. A.; Fahie, B. J.; Lyerla J. R., et al. *Macromolecules* **1992**, *25*, 1623.
(27) Lyerla, J. R.; Economy, J.; Maresch, G.; Muhlebach, A.; Yannoni, C. S.; Fyfe, C. A. *Polym. Prepr. (Am. Chem. Soc., Div. Polym. Chem.)* **1988**, *30*, 534.
(28) Clements, J.; Humphreys, J.; Ward, I. M. *J. Polym. Sci., Polym. Phys.* **1986**, *24*, 2293.
(29) Dynamic mechanical studies (ref 30), which reported a split primary, α, glass transition at low frequencies (refs 30 and 31), were omitted for simplification only.
(30) Wissbrun, K. F.; Yoon, H. N. *Polymer* **1989**, *30*, 2193.
(31) Devens, D. A., Jr.; Denn, M. M. *Polym. Adv. Tech.* **1995**, *6*, 693.
(32) Jonscher, A. K. *Dielectric relaxation in solids*; Chelsea Dielectrics: London, 1983.
(33) Kaito, A.; Kyotani, M.; Nakayama, K. *Macromolecules* **1990**, *23*, 1035.
(34) Havens, J. R.; VanderHart D. L. *Macromolecules* **1985**, *18*, 1663.
(35) Cheung, T. T. P.; Gerstein, B. C. *J. Appl. Phys.* **1981**, *52*, 5517.
(36) Bryngelson, J. D.; Wolynes, P. G. *Proc. Natl. Acad. Sci. U.S.A.* **1987**, *84*, 7524.
(37) Abkevich, V. I.; Gutin, A. M.; Shakhnovich, E. I. *Biochemistry* **1994**, *33*, 10026.
(38) Wunderlich, B.; Moeller, M.; Grebowicz, J.; Buar, H. *Adv. Polym. Sci.* **1988**, *87*, 1.
(39) VanderHart D. L.; Orts, W. J.; Marchessault, R. H. *Macromolecules* **1995**, *28*, 6394.
(40) Barker, P. A.; Barham, P. J.; Martinez-Salazar, J. *Polymer* **1997**, *38*, 913.
(41) Extrapolation of melt *trans*-esterification rates at 315 °C, using a 152 kJ/mol activation energy (ref 42) to the solid state, at 285 or 255 °C, would not rule out significant reaction in the annealing times used. However, reaction in the solid is likely to proceed considerably more slowly. Also, *trans*-esterification in miscible HBA/HNA copolyester blends has been observed to occur only with application of high pressure an order of magnitude larger than the overpressure used in this study (refs 42 and 43). Most importantly, the expected result of crystallization-directed *trans*-esterification would be large (≫10 nm), high-melting-temperature homopolymer crystals, which have not been observed in the HBA/HNA system here or elsewhere (refs 6 and 8).
(42) McCullagh, C. M.; Blackwell, J.; Jamieson, A. M. *Macromolecules* **1992**, *25*, 1623.
(43) Muhlebach, A.; Economy, J.; Johnson, R. D.; Karis, T.; Lyerla, J. *Macromolecules* **1990**, *23*, 1803.
(44) Kroemer, H.; Kuhn, R.; Pielartzik, H.; Siebke, W.; Eckhardt, V.; Schmidt, M. *Macromolecules* **1991**, *24*, 1950.

(45) An extrapolated melting enthalpy for 75/25 poly(HBA/HNA) for "infinite crystallization time" has been reported to be 3.7 kJ/mol (ref 6), based on an average monomeric molecular weight of 132.5. If we consider the relevant chain unit to be a persistence length, the relevant molecular weight consists of ~15 average monomeric units (based on 0.64 and 0.84 nm HBA and HNA unit lengths, respectively, and a 10-nm persistence length). The renormalized melt enthalpy becomes 55 kJ/mol, close to the usual 20−50 kJ/mol observed in more flexible systems.
(46) Hanna, S.; Windle, A. H. *Polymer* **1988**, *29*, 207.
(47) Löffler, R.; Novaro, P. *Macromolecules* **1992**, *28*, 7172.

MA961109N